Structural, Electronic, and Chemical Properties of Nanoporous Carbon

Johan M. Carlsson* and Matthias Scheffler†

Fritz-Haber-Institut der Max-Planck-Gesellschaft, Faradayweg 4-6, D-14195 Berlin, Germany

(Received 24 March 2005; published 3 February 2006)

Nanoporous carbon (NPC) exhibits unexplained chemical properties, making it distinct from other graphenelike materials, such as graphite, fullerenes, or nanotubes. In this Letter, we analyze the properties of NPC in terms of its structural motifs, which are derived from defects in distorted graphene sheets. Our density-functional theory calculations show that these motifs can be present in high concentration (up to 1%). Some of them induce localized levels close to the Fermi level, therefore leading to local charging and controlling the material's chemical function, for example, as a catalyst.

DOI: 10.1103/PhysRevLett.96.046806 PACS numbers: 81.05.Uw, 61.72.Ji, 73.22.-f, 82.75.-z

Carbon has the unique capability of forming a variety of interesting materials exhibiting extraordinarily different physical and chemical properties. Fullerene, carbon-nanotubes, graphite, and diamond are examples. Experimentally, it is known that harsh treatment such as electron irradiation [1], ion bombardment [2], or plasma oxidation [3] is necessary to create defects in these systems. This has led to the common belief that uncontaminated carbon materials have low defect concentration and that they are more or less chemically inert. In conflict with this view, experimental work recently revealed that certain carbon structures can be catalytically active [4,5]. The atomic structure of this novel catalyst material is still unknown, but there is evidence that the material has a nanoporous structure. Such nanoporous carbon (NPC) constitutes an intermediate class of carbon materials which are less ordered than graphite, but still not completely amorphous. There exists a variety of NPC materials and the actual structure depends on the preparation conditions and the starting material. In this Letter we concentrate on NPC derived from hydrocarbons and transmission electron microscopy (TEM) studies showing that NPC produced by arc discharge [6] or carbonization of sucrose [7] takes the form of fullerene fragments. Neutron diffraction experiments [8] indicate that pyrolysis of Polyfurfuryl alcohol (PFA) provides NPC in the form of curved, defective graphene sheets. Corresponding simulations [9,10] reveal that it is necessary to include nonhexagonal rings in the model to obtain reasonable agreement with the neutron diffraction data. This suggests that there are distinct motifs present in most forms of NPC although the overall structure of these materials might be quite different.

We have therefore made a detailed theoretical study of motifs that have been suggested to appear in NPC materials [6–10]. We define these motifs in terms of combinations of nonhexagonal rings that appear due to defects in the graphene lattice. The aim is also to generalize the understanding of how defects affect the properties of sp^2 bonded carbon networks present in graphite, fullerenes, and nanotubes. We find that motifs derived from vacancies are the most likely candidates to control the material's chemical properties. The heat of formation H_{NPC} for this model of NPC is comparable to, or even more favorable than, that of carbon nanotubes even when the concentration of these motifs is as large as $\approx 1\%$. We furthermore find that these motifs introduce a defect state close to the Fermi level. This can lead to charging and facilitate the dissociation of approaching molecules.

We used density-functional theory (DFT) [11,12] together with the generalized gradient approximation for the exchange-correlation functional [13]. Two different computer codes were employed to ensure that there are no numerical artifacts, in particular, when dealing with strained and charged systems. The FHI98MD code [14] uses norm-conserving pseudopotentials and a plane-wave basis set with an energy cutoff of 50 Ry. The DMOL^3 code [15] is an all-electron code with atom-centered, numerical basis functions that are cutoff at 12 bohr. Both codes gave essentially the same lattice parameter for graphene, $a = 2.46$ Å, with a difference below 0.01 Å. We modeled the motifs as defects in a graphene sheet by a supercell approach. The rectangular unit cell of graphene [cf. the dashed line in Fig. 1(a)] has been extended (4×7) times such that the supercell contains 112 atoms for perfect graphene. The sheet separation is 17 Å, which ensures that the sheet-sheet interaction is negligible. The Brillouin zone was sampled with a $(6 \times 6 \times 1)$ mesh. The lattice parameters were varied to study the effect of strain, and the atomic positions were relaxed until the maximal force/atom was smaller than 0.02 eV/Å. The formation energy of a structural motif is

$$E_{\mathrm{form}}(\mu_{\mathrm{C}}, q, \epsilon_{\mathrm{F}}) = \{E^{\mathrm{motif}}(n_{\mathrm{C}}, q) + n_{\mathrm{C}}\mu_{\mathrm{C}}\} - E^{\mathrm{G}} + q\epsilon_{\mathrm{F}}, \quad (1)$$

where E^{G} and E^{motif} refer to the total energy of a graphene sheet before and after the defect is created, n_{C} denotes the number of C atoms that has been exchanged with the reservoir μ_{C}, q is the charge state of the defect, and ϵ_{F} is the Fermi level in the system. Charged defects were calculated using a compensating jellium background, which was

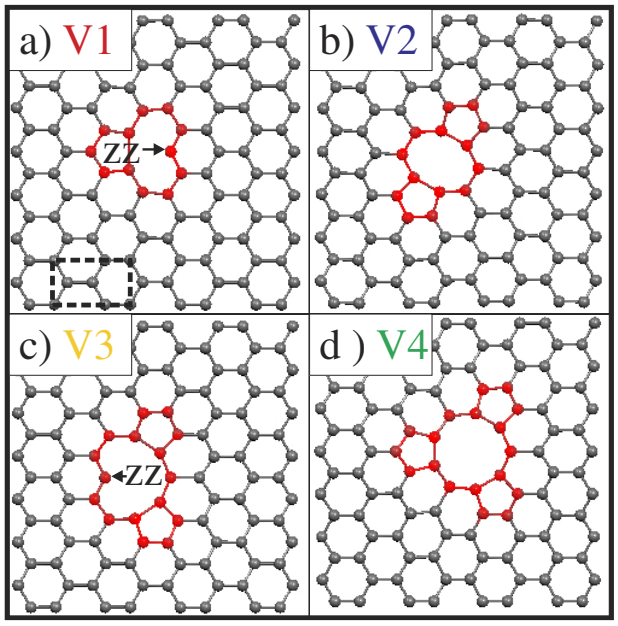

FIG. 1 (color online). Atomic structures of various NPC motifs (fully relaxed). The atoms that are part of the nonhexagonal region are colored red. Panel (a) also gives the unit cell of a graphene sheet (dashed lines). The left panels (a),(c) show defect structures with an odd number of removed atoms: (a) single vacancy (V1), and (c) trivacancy(V3). Undercoordinated atoms are labeled as "ZZ" (zigzag atom). Panels at the right show defects with an even number of removed atoms: (b) divacancy (V2) and (d) quadrovacancy (V4).

estimated to give a less than 0.1 eV error contribution to the total energy.

Small defects in graphite such as C adatoms [16,17], the 5-7-5-7 defect [called Stone-Wales (SW) defect [18]], and the single vacancy [2,19–24] have been studied extensively. Larger defects have been considered in the context of radiation damage [25] and nonhexagonal rings as the origin of negative curvature in Schwarzites [26,27]. However, defects have not been studied in connection with the chemical properties of NPC previously.

Our calculations reveal that the atoms in the neighborhood of a vacancy rearrange to reduce the number of dangling bonds as can be seen in Fig. 1. Incomplete hexagons transform into irregular pentagons and the atoms surrounding the vacancy rebond into a large *vacancy ring* containing N_{ring} atoms. The bond lengths in the vacancy ring vary between 1.42 and 1.8 Å, and are thus up to 30% longer than in perfect graphene. This reflects that the bonds in the vacancy ring are strained and weaker than in a pure sp^2 hybridization. The atomic relaxations at defects consequently result in the formation of motifs, which are combinations of nonhexagonal rings. The bond angles do in general not sum up to 360° at vertices where there are nonhexagonal rings present. The carbon atoms can compensate for this deviation either by adjusting the bond angles or by bending the lattice when the deviation is larger. The relaxation therefore leads to extended rearrangement of the atoms surrounding the defect, which broadens the calculated radial distribution function (RDF). This supports the interpretation of the neutron diffraction measurements of NPC that the strong deviation compared to graphite originates from nonhexagonal rings in the structure [8]. Euler's rule [26] gives a relation between the number of nonhexagonal rings in the lattice and the character of the surface in terms of the topological genus g. A fullerene of $g = 0$ has 12 pentagons, as an example. We can furthermore derive a condition for the combination of nonhexagonal rings, which states that the genus of the surface is preserved when *the number of excess atoms in the vacancy ring equals the number of surrounding pentagons*:

$$N_{\text{pentagons}} = N_{\text{ring}} - 6. \tag{2}$$

We can now divide the defects in Fig. 1 into *even* and *odd* defects. The even defects in the right column are fully rebonded and conform to Eq. (2). Within the limitations of the supercell approach, the even defects are therefore just locally buckled around the defect. The odd defects in the left column have one remaining undercoordinated C atom after relaxation in a configuration similar to the atoms on the zigzag edge of the graphene sheet. These "zigzag" atoms shorten the bond length to the two neighboring C atoms by approximately 0.05 Å and have a remaining dangling bond. The Jahn-Teller distortion observed at the single vacancy [19,22,24] is therefore a special case of the symmetry-lowering rebonding relaxation at the odd vacancies.

Comparing the formation energies for the odd and even vacancies, which are summarized in Fig. 2, indicates that the remaining zigzag atom at the odd vacancies is highly unfavorable. The odd ($2m - 1$, m = integer) and corresponding larger ($2m$) even vacancies have nearly the same formation energies in the region where μ_C is close to the value in graphene (cf. the V1 and V2 in Fig. 2). This indicates that the zigzag atom can be removed without any energy cost forming the next, larger, even vacancy during growth in a graphitic environment.

A somewhat puzzling aspect for describing NPC is that the formation energies of all defects considered here (cf. Fig. 2) are so large that the equilibrium concentration is completely negligible. However, it is well known that free energy barriers are significant in carbon systems and that fullerenes or nanotubes are in fact just metastable structures in comparison to graphite. Nevertheless, all these forms of carbon have a considerable lifetime. Thus, we will compare the heat of formation of NPC to that of nanotubes assuming that the NPC material resides in a metastable state once it has been created. We are here modeling NPC as graphene sheets with a varying amount of motifs of the type shown in Fig. 1. These motifs can be considered to have formed during the growth of the mate-

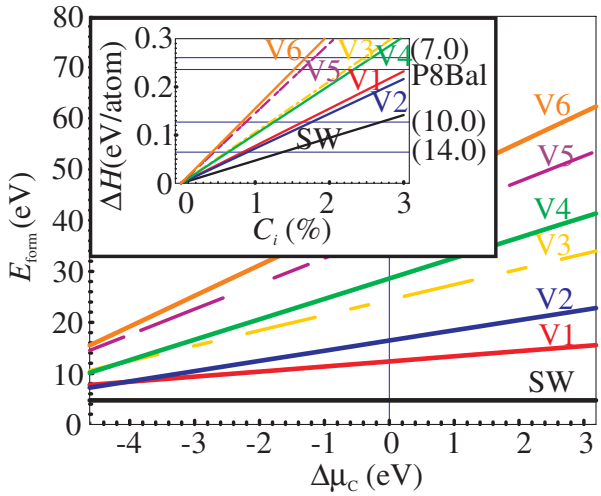

FIG. 2 (color online). Formation energies, E_{form}, for defects in a graphene sheet as function of $\Delta\mu_C = \mu_C - 1/2E_{C_2}$. The right limit is the free C atom at $T = 0$ K and the left limit is μ_C of graphene at $T = 0$ K. The vertical line at $\Delta\mu_C = 0$ corresponds to the energy of a carbon atom in a C_2 molecule at zero temperature. The labels refer to the SW defect, and the vacancy (V1) and vacancy clusters (from V2 to V6). The inset shows the heat of formation/atom of NPC compared to graphene: $\Delta H = H_{\text{NPC}} - H_{\text{G}}$ as function of the defect concentration. The horizontal lines give ΔH for three zigzag nanotubes of different diameters (7, 0), (10, 0), and (14, 0) and the P8Bal model of NPC [27].

rial due to lattice mismatch or evaporation of noncarbon atoms. The heat of formation of NPC, H_{NPC} with a certain concentration C_i of motif (i) is

$$H_{\text{NPC}}(C_i) = H_{\text{G}} + \sum_i C_i E^i_{\text{form}}(\mu^{\text{G}}_{\text{C}}), \qquad (3)$$

where H_{G} is the heat of formation per atom for graphene and $E^i_{\text{form}}(\mu^{\text{G}}_{\text{C}})$ is the formation energy of the defect in graphene. The inset in Fig. 2 shows that our NPC models with a concentration of motifs up to 1% yield H_{NPC} comparable to single wall zigzag nanotubes. It is also lower than the P8Bal structure, which is reported to be the most stable of the Schwarzite models for NPC [27]. This indicates that a graphene sheet can have a moderate amount of voids, such as the motifs in Fig. 1, and still be metastable as long as the barriers towards graphitization are large enough. This is in agreement with the conclusions from TEM [6,7] and neutron diffraction experiments [8] that NPC derived from hydrocarbons has the form of defective graphene sheets.

These motifs have a significant influence on the electronic structure of NPC, such that new states appear, which are not present in the density of state (DOS) for pristine graphene. The absence of atoms in the void and the atomic rearrangement perturb the alignment of the p_z orbitals forming the π band. This splits off a p_z state from the π band as can be seen as an additional peak in the DOS close to the Fermi level in graphene $\epsilon^{\text{G}}_{\text{F}}$ for all the motifs considered in Fig. 3. The wave function for this p_z state is semilocalized around the motif and it has the largest amplitude on the C atoms surrounding the void. The motifs derived from odd vacancies have in addition a dangling bond (DB), connected to the undercoordinated zigzag atom. The DB state appears in the band gap between the occupied and unoccupied σ band. The DB state is therefore localized to the zigzag atom and becomes completely spin polarized. The DB state is clearly visible in the DOS for the V1 motif in Fig. 3 as a peak in the spin-up channel, 1 eV below $\epsilon^{\text{G}}_{\text{F}}$. We have also observed a similar DB state connected to the zigzag atom at other odd motifs such as the V3 and V5.

The integrated difference DOS in the lower panel of Fig. 3 reveal that the defects change the population of the electronic states such that the additional states are occupied at motifs derived from vacancies. Comparing the upper and lower panel indicates furthermore that these additional electrons are trapped in the p_z-state. Hückel calculations also indicate that an extra π electron is associated with a single vacancy [21]. We have therefore made a charge state analysis of the even motifs shown in Fig. 4. This reveals that the intrinsic charge state of the SW motif is neutral, while the motifs derived from vacancies would be negatively charged. This can be connected to the gradual low-

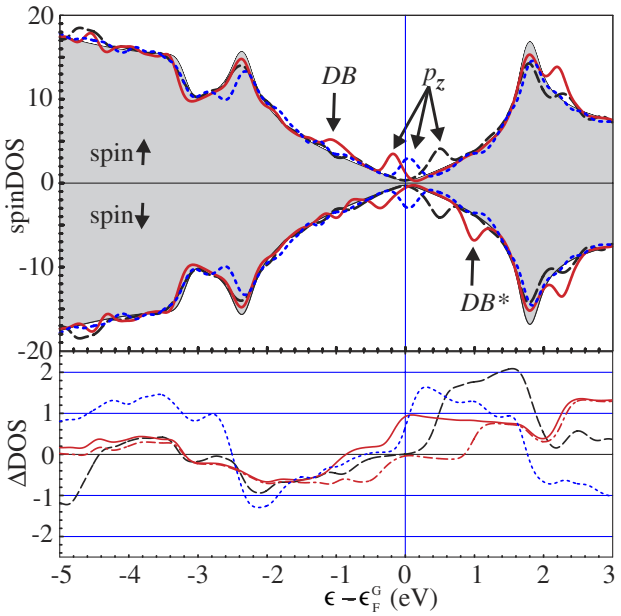

FIG. 3 (color online). Upper panel: Spin polarized density of states (spin DOS) for a graphene sheet with a SW defect (black dashed line), single vacancy V1 (red solid line), and divacancy V2 (blue dash-dotted line). The gray shaded regions show the DOS for perfect graphene and the energy scale is set to zero at $\epsilon^{\text{G}}_{\text{F}}$, which is indicated by the vertical line. The arrow marked DB marks the positions of the dangling bond state and p_z shows the position of the p_z state. Lower panel: the integrated difference DOS (ΔDOS) for the same defects.

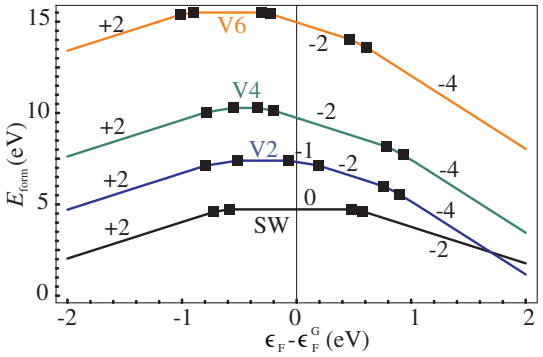

FIG. 4 (color online). Formation energy $E_{\text{form}}(\epsilon_F)$ for the even defects as function of the Fermi level ϵ_F in the system, which is given relative to perfect graphene, ϵ_F^G. The numbers indicate the charge state and the black dots indicate the position of the charge transfer levels. The intrinsic charge state for the defects is given by the value at ϵ_F^G.

ering of the energy for the p_z state. Figure 3 shows that the p_z state is unoccupied at the SW motif, while it coincides with ϵ_F^G for the V2 motif. Our calculations also show that the p_z state lies completely below ϵ_F^G for the V4 and V6 motifs. The charging of these motifs agrees with the STM observation of an increased signal around vacancies in sputtered graphite [2]. Additional STM measurements show that charging of graphite by Cs doping increase the reactivity towards oxidation [28], which suggests that the local charging of the motifs would increase the reactivity towards electronegative molecules such as oxygen. The motifs are also more receptive to adsorption because the strained bonds in the vacancy ring are weaker than the bonds in the basal plane. An increased activity of the motifs agrees also with the observation that O_2 molecules preferentially dissociate at vacancies in graphite [3].

In summary, our results together with previous simulations [9,10] and experimental work [6–8] suggest that NPC, or at least regions of it, can be described in terms of graphene sheets with voids frozen in during the growth phase of the material. Atomic relaxation forms a combination of nonhexagonal rings that leads to a local buckling around the motif. The heat of formation for this model of NPC is comparable to that of single-wall nanotubes, which indicates that NPC will be metastable as long as the chemical environment is gentle enough to prevent graphitization or burning. We propose that the increased chemical activity of NPC is connected to these motifs. The additional charge at the motifs can assist the dissociation of adsorbing molecules and it is easier for the molecules to attach to the atoms around the void. The dissociative adsorption of molecules such as oxygen could in turn modify the chemical properties by forming functional groups, which is the subject of a further study.

The authors would like to thank S. Linic, R. Schlögl, and D. Su for fruitful discussions.

*Electronic address: johanc@fhi-berlin.mpg.de
†Electronic address: scheffler@fhi-berlin.mpg.de

[1] A. Hashimoto, K. Suenaga, A. Gloter, K. Urita, and S. Iijima, Nature (London) **430**, 870 (2004).
[2] J. R. Hahn, H. Kang, S. Song, and I. C. Jeon, Phys. Rev. B **53**, R1725 (1996).
[3] J. I. Paredes, A. Martinez-Alonso, and J. M. D. Tascón, Carbon **38**, 1183 (2000).
[4] M. S. Kane, L. C. Kao, R. K. Mariwala, D. F. Hilscher, and H. Foley, Ind. Eng. Chem. Res. **35**, 3319 (1996).
[5] G. Mestl, N. I. Maksimova, N. Keller, V. V. Roddatis, and R. Schlögl, Angew. Chem., Int. Ed. Engl. **40**, 2066 (2001).
[6] L. N. Bourgeois and L. A. Bursill, Philos. Mag. A **76**, 753 (1997).
[7] P. J. F. Harris, A. Burian, and S. Duber, Philos. Mag. Lett. **80**, 381 (2000).
[8] V. Petkov, R. G. DiFrancesco, S. J. L. Billinge, M. Acharaya, and H. C. Foley, Philos. Mag. B **79**, 1519 (1999).
[9] M. Acharaya *et al.*, Philos. Mag. B **79**, 1499 (1999).
[10] M. A. Smith, H. C. Foley, and R. F. Lobo, Carbon **42**, 2041 (2004).
[11] P. Hohenberg and W. Kohn, Phys. Rev. **136**, B864 (1964).
[12] W. Kohn and L. J. Sham, Phys. Rev. **140**, A1133 (1965).
[13] J. P. Perdew, K. Burke, and M. Ernzerhof, Phys. Rev. Lett. **77**, 3865 (1996).
[14] Computer code FHI98MD: M. Bockstedte, A. Kley, J. Neugebauer, and M. Scheffler, Comput. Phys. Commun. **107**, 187 (1997).
[15] Computer code DMOL^3, Academic version: B. Delley, J. Chem. Phys. **92**, 508 (1990).
[16] K. Nordlund, J. Keinonen, and T. Mattila, Phys. Rev. Lett. **77**, 699 (1996).
[17] P. O. Lehtinen, A. S. Foster, A. Ayuela, A. Krasheninnikov, K. Nordlund, and R. M. Nieminen, Phys. Rev. Lett. **91**, 017202 (2003).
[18] A. J. Stone and D. J. Wales, Chem. Phys. Lett. **128**, 501 (1986).
[19] A. Zunger and R. Englman, Phys. Rev. B **17**, 642 (1978).
[20] E. Kaxiras and K. C. Pandey, Phys. Rev. Lett. **61**, 2693 (1988).
[21] M. Hjort and S. Stafström, Phys. Rev. B **61**, 14 089 (2000).
[22] A. A. El-Barbary, R. H. Telling, C. P. Ewels, M. I. Heggie, and P. R. Briddon, Phys. Rev. B **68**, 144107 (2003).
[23] C. P. Ewels, R. H. Telling, A. A. El-Barbary, M. I. Heggie, and P. R. Briddon, Phys. Rev. Lett. **91**, 025505 (2003).
[24] Y. Ma, P. O. Lehtinen, A. S. Foster, and R. M. Nieminen, New J. Phys. **6**, 68 (2004).
[25] A. V. Krasheninnikov, K. Nordlund, and J. Keinonen, Phys. Rev. B **65**, 165423 (2002).
[26] H. Terrones and A. L. Mackay, Carbon **30**, 1251 (1992).
[27] F. Valencia, A. H. Romero, E. Hernandez, M. Terrones, and H. Terrones, New J. Phys. **5**, 123 (2003).
[28] J. R. Hahn and H. Kang, J. Phys. Chem. B **106**, 7445 (2002).